Int. J. Heat Mass Transfer. Vol. 36, No. 2, pp. 391–399, 1993
Printed in Great Britain

0017-9310/93 $6.00+0.00
Pergamon Press Ltd

Thermal processes under the action of laser radiation pulse on absorbing granules in heterogeneous biotissues

V. K. PUSTOVALOV
Byelorussian Polytechnical Institute, 220027, Minsk, Belarus

(*Received* 9 *January* 1992)

Abstract—Energy absorption, heat transfer and thermodenaturation, as well as thermomechanical processes and vapour generation, under the action of laser radiation pulse on pigmented spherical granules in heterogeneous laminated biotissues are investigated theoretically. A system of equations is formulated and, based on its numerical solution, consideration is given to the formation and dynamics of a vapour blanket originating during the radiation pulse interaction with an absorbing granule in a water-containing biotissue. The values of radiation pulse energy are calculated which give rise to granular and ophthalmoscopically visible thermodenaturation lesions on the retina and to vapour generation on granules in the pigmented epithelium. A comparison and agreement of numerical results with experimental data validate the models and techniques developed.

1. INTRODUCTION

THE INVESTIGATION of the interaction of laser radiation pulses with heterogeneous laminated biotissues is of exceptional interest for photobiology and laser medicine as well as for determining scientifically justified safety norms to handle intense laser radiation sources [1, 2]. Particular attention is called to investigations of radiation pulse interaction with tissues of the eye as the organ most vulnerable to radiation damage owing to a wide use of lasers in ophthalmology. As follows from experimental results [1, 2], the most practically important mechanism is the thermal nonresonance action inducing heating, heat transfer and other thermal processes. One of the eye biotissue layers, namely the pigmented epithelium (PE), contains spherical and spheroidal pigmented melanoprotein granules of characteristic sizes of about 1 μm. In this case, the granules selectively absorb up to 90% of radiation energy, absorbed throughout the PE layer [3], whereas the surrounding biotissues have a markedly smaller absorptivity. During irradiation, the granules absorb energy, become overheated relative to the surrounding biotissues and exchange heat by the mechanism of heat conduction with the ambience. Studies [4, 5] ascertained the possibility of selective thermodenaturation of the melanoprotein granules by radiation pulses of duration $t_p < 10^{-3}$ s and of definite energy $Q_{c.g}$ which consists of the formation of a thermodenaturation lesion localized inside and around the granules without origination of a continuous macroscopic thermodenaturation lesion. The current study calculated the energy values resulting in the formation of granular ($Q_{c.g}$) and ophthalmoscopically visible ($Q_{c.o}$) thermodenaturation lesions. With an increase in radiation pulse energy (intensity), thermal processes other than heat transfer and thermodenaturation also arise in the biotissues. This is verified by experimental data [6, 7] indicating the emergence of biotissue damage with an energy increase which manifests itself in eye tissue ruptures, hemorrhages, etc. Of special interest is clarification of the physical mechanisms inducing mechanical stresses in the pigmented biotissues by the action of radiation pulses. Since the granules are the main radiation energy absorbers in the pigmented layers (PE) the processes with the lowest energy threshold will, apparently, be initiated on the granules. Below, a rapid heating, thermal expansion and thermomechanical processes in the biotissues without phase transition are examined. A system of equations is also formulated and, based on its numerical solution, consideration is given to the formation and dynamics of a vapour blanket originating during the radiation pulse interaction with the absorbing granule in the water-containing biotissue. Numerical results are compared with experimental data.

2. THERMAL PROCESSES IN THE PIGMENTED EYE TISSUES UNDER THE ACTION OF RADIATION PULSES

Studies [4, 5] have formulated a system of equations and determined the techniques for its numerical solution. This enables predictions of the action of radiation pulses with $t_p \lesssim 10^{-3}$ s on the eye tissue, taking into account the granular PE structure, and production of the pattern of energy absorption, heating and heat transfer as well as that of thermodenaturation both around individual granules and for the entire biotissue volume in question. Thermodenaturation is a heating-induced breakdown of the protein macromolecular structure, resulting in the loss of natural functional properties by protein [8] and in biotissue damage. This section gives the results

NOMENCLATURE

c	heat capacity of biotissue (medium)
c_0	heat capacity of granule material
D_r	diameter of irradiation spot on retina
f	thermodenaturation degree of protein molecules
ΔH	difference of enthalpies of initial and activated states
I	radiation intensity
I_0	maximum radiation intensity on beam axis
j	mass flux density of vapour
K_{ab}	efficiency factor of radiation energy absorption by granule
m_2	mass of water molecule
M	mass
p	pressure
Q_c	radiation pulse energy on cornea
$Q_{c.g}$	radiation pulse energy causing the generation of granular thermodenaturation lesion
$Q_{c.o}$	radiation pulse energy causing ophthalmoscopically visible thermodenaturation lesion on retina
$Q_{c.v}$	radiation pulse energy causing vapour generation on granules
R_b	characteristic beam radius
R_g	gas constant
r	radial coordinate with origin fixed at granule centre
ΔS	difference of entropies of initial and activated states
T	temperature
T_0	temperature within granule
T_∞	initial temperature
t	time
t_p	pulse duration
V	volume
V_0	volume of granule
v	rate.

Greek symbols

α_{ev}	condensation (evaporation) coefficient of water
γ	adiabatic exponent of water vapour
κ	thermal conductivity
λ	radiation wavelength
ν	kinematic viscosity
ρ	density
ρ_0	density of granule material
σ	surface tension
χ	thermal diffusivity.

Subscripts

$i = 0$	particle
$i = 1$	vapour
$i = 2$	liquid (biotissue).

predicted from the model [4, 5] for the threshold energies $Q_{c.g}$, $Q_{c.o}$.

The radiation intensity distribution across the beam section is taken to be Gaussian

$$I(X = 0) = I_0(t) \exp(-R^2/R_b^2) \qquad (1)$$

where $I_0 = I(X = 0, R = 0, t)$ is the maximum beam axial intensity on the cornea, and R_b is the characteristic beam radius. The time dependence of the intensity during the pulse is selected to be Gaussian of the pulse duration t_p with an intensity level of $0.5I_0$. Here, pulse energy on the cornea Q_c, in view of the Gaussian dependences of I on time and radius for an infinite beam, is defined by the expression

$$Q_c = \int_0^\infty dt \int_0^\infty I(X = 0) 2\pi R \, dR. \qquad (2)$$

For a rectangular dependence of I on t and an infinite Gaussian beam, $Q_c = I_0 \pi R_b^2 t_p$.

The threshold radiation pulse energy $Q_{c.o}$, measured on the cornea, is generally understood as energy by the action of which on the retina an ophthalmoscopically visible thermodenaturation lesion emerges, represented as greyish-white spots of the characteristic size equal to about 20–30 μm, visible with an ophthalmoscope with a probability of 50% on the eyeground (retina) immediately or not long after exposure [6]. The predominant influence of thermodenaturation on the processes of retina biotissue damage under the action of radiation pulses with threshold energy values is proved by histological investigations of the biotissues after exposure [6] and by agreement between the threshold energies, calculated assuming that the biotissue damage is caused by thermodenaturation, and the experimental threshold energies [9, 10]. Since medical experiments usually use laboratory animals, calculations were performed for the processes of the interaction of radiation pulses with $\lambda = 1.06$ μm, a duration of $10^{-3} \gtrsim t_p \gtrsim 10^{-8}$ s and a Gaussian intensity distribution across the beam section with a rabbit retina for the purpose of comparing calculated results with experimental data [6]. Geometrical and optical (for a medium pigmentation) parameters of the rabbit eye media are taken from ref. [10]. Inasmuch as the experiment [6] has not determined the size of the irradiation spot on the retina, the characteristic spot radius $R_{s.r} \approx 50$ μm was obtained numerically, such that the sizes of the thermodenaturation lesion predicted conform to the experimental values. In this case, the calculated threshold energy $Q_{c.o}$ is understood to be the energy causing the formation of the ophthalmoscopically visible ther-

modenaturation lesion on the PE (retina) about 25 μm in diameter by the thermodenaturation degree of the protein molecules $f = 0.5$ (the initial value is $f = 1$), i.e. the fraction of thermoinactivated protein molecules within the thermodenaturation lesion is larger than 50%. In the numerical calculations, the reverse problem is solved, i.e. the pulse energy is selected such that the sizes of the originating thermodenaturation lesions deviate minimally from those of the ophthalmoscopically visible thermodenaturation lesions.

Since, during irradiation, the granules are heated to temperatures higher than those of the surrounding biotissues, then owing to a pronounced temperature dependence of thermodenaturation, the case can be realized by selecting radiation energy (intensity) where thermodenaturation only occurs within or near the granular surface, i.e. a granular thermodenaturation lesion is formed. In the given case, the granular thermodenaturation lesion is assumed to be the thermodenaturation lesion located inside and near melanoprotein granules with the thermodenaturation degree on the granule surface constituting $f = 0.5$, i.e. the fraction of thermoinactivated molecules within the granule is in excess of 50%. Here, the thermodenaturation microregions do not overlap and so do not set up a continuous thermodenaturation lesion in the retina biotissues. This possibility of a selective thermodenaturation of the pigmented biotissues by radiation pulses of $t_p \leqslant 10^{-3}$ s and certain energies $Q_{c.g}$ was established from the numerical simulation in refs. [4, 5]. The selective irradiation is realized in this case at energy $Q_{c.g}$ levels 2–5 times smaller than the threshold pulse energy $Q_{c.o}$ which induces the formation of the ophthalmoscopically visible thermodenaturation lesion.

Figure 1 presents the experimental [6] and numerical results for the threshold energies $Q_{c.o}$ and $Q_{c.g}$ of radiation pulses on the rabbit cornea. The experimental values ($\dot{\varphi}$) and (Δ) correspond to the energies causing the threshold ophthalmoscopically visible retina damage with probabilities of 50 and 0.1%, respectively. The predicted energies $Q_{c.o}$ and $Q_{c.g}$ conform to the formation of the ophthalmoscopically visible ($Q_{c.o}$) and granular ($Q_{c.g}$) thermodenaturation lesions. It should be noted that, at $t_p = 10^{-3}$, 10^{-4}, here and hereafter a constant I_0 value is employed in calculations for $0 < t \leqslant t_p$. A satisfactory agreement between the experimental and theoretical values of the energy $Q_{c.o}$ is obtained. The energies $Q_{c.o}$ and $Q_{c.g}$ calculated at $t_p = 10^{-3}$ s actually coincide, as was remarked in ref. [5]. A generality of the 3–10 fold decrease in the energies $Q_{c.o}$, $Q_{c.g}$ with a reduction in the pulse duration t_p from 10^{-3} to 10^{-7} s is observed. Within the range $10^{-9} < t_p \leqslant 10^{-7}$ s, $Q_{c.o}$ and $Q_{c.g}$ are virtually invariable. A physical reason for such a dependence of $Q_{c.o}$ and $Q_{c.g}$ on t_p is the following. The characteristic time of heat transfer for the granule of $r_0 = 1$ μm, is $t_1 \approx r_0^2/4\chi = 1.6 \times 10^{-6}$ s, where $\chi = 1.73 \times 10^{-2}$ cm^2 s^{-1} [11] is the thermal diffusivity

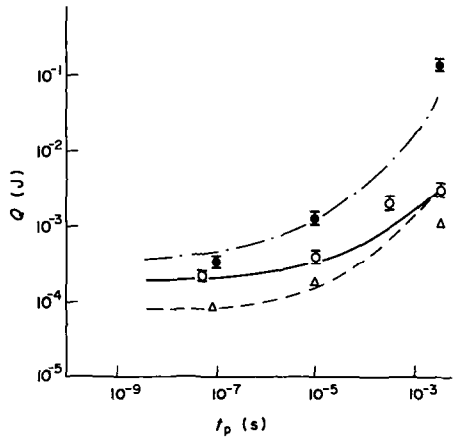

FIG. 1. The dependences of the calculated energies $Q_{c.v}$ (·—·—·), $Q_{c.o}$ (——), $Q_{c.g}$ (– – –) of radiation pulses with $\lambda = 1.06$ μm on the rabbit cornea on t_p at the diameter of the irradiation spot on the retina $D_r = 2R_{s.r} \approx 100$ μm. Experimental energy values [6]: ($\dot{\varphi}$) pulse energy causing subretinal hemorrhage with probability 50%; ($\dot{\varphi}$) and (Δ) pulse energies causing threshold retina damage with probabilities of 50 and 0.1%.

of the PE tissues. The characteristic time of heat removal from the PE of thickness l_{PE} equal to about 5 μm is $t_2 \sim l_{PE}/4\chi = 4 \times 10^{-5}$ s. When radiation pulses of $t_p < t_1$ and t_2 are acting, the granules and biotissue become heated virtually without heat removal during the pulse action beyond the irradiation spot and $Q_{c.o}$, $Q_{c.g} \approx$ const. within the range $10^{-9} < t_p \leqslant 10^{-7}$ s. An increase in t_p at $t_p > t_1$, t_2 results in a noticeable enhancement of heat removal during irradiation as well as in an increase of $Q_{c.o}$ and $Q_{c.g}$ needed for reaching a definite heating temperature of the biotissue and a thermodenaturation degree. When radiation pulses of $t_p > 10^{-3}$ s are acting, the radiative heating of the granules takes place at an intense heat exchange; here, the granule overheating relative to the environment tends to zero and the threshold energies for ophthalmoscopic $Q_{c.o}$ and granular $Q_{c.g}$ thermodenaturation lesions actually coincide.

According to Fig. 1, there is a certain correlation between the experimental (Δ) and predicted energies $Q_{c.g}$. A ratio of the threshold energies $\dot{\varphi}/\Delta$, $Q_{c.o}/Q_{c.g}$ for $t_p \sim 10^{-6}$ s runs into about 2–4. Following ref. [6], the region of clinically subthreshold energies between the values $\dot{\varphi}$ and Δ (and, correspondingly, between $Q_{c.o}$ and $Q_{c.g}$) can be regarded as the region of functional changes in the retina tissues. The energy range indicated can be used in practical laser ophthalmology to achieve a curing effect on transition from laser biostimulation and selective thermodenaturation of the PE granules to laser thermodenaturation (coagulation) of the retina tissues. Besides determining the threshold energies $Q_{c.g}$ for thermodenaturation of the PE granules, which are considerably (about 2–4 times) smaller than the threshold energies $Q_{c.o}$ for the ophthalmoscopically visible lesion, it is important in specifying the safety norms of laser radiation for the

retina. Here, $Q_{c.g}$ can serve as a complementary insuring parameter in setting up the safety norms. A comparison is carried out between the radii of the continuous ophthalmoscopic denaturation lesion R_0 calculated by the thermodenaturation degree $f = 0.5$ for the experimental [6] and predicted energies $Q_{c.o}$ and various t_p. The R_0 values obtained from the conditions [6] amount, on average, to $R_0 \sim 30$–40 μm; in this case, the maximum temperatures of the eyeground biotissue are $T_m \sim 363$–378 K. The R_0 values predicted using the theoretical $Q_{c.o}$ values are equal, on average, to $R_0 \sim 12.5$–15 μm with the maximum biotissue temperature here being $T_m \sim 360$–372 K.

Calculations are accomplished for the processes of the interaction of radiation pulses of $\lambda = 1.06$ μm, a duration range of $10^{-3} > t_p > 10^{-9}$ and a Gaussian intensity distribution across the beam section with monkey retina tissues for the aim of comparing predictions with experimental data [12]. Geometrical and optical parameters of the monkey eye media are taken from ref. [10], whereas variations in the enthalpy ΔH and entropy ΔS of the retina proteins during thermodenaturation are taken from refs. [9, 13]. In view of the fact that the experiment [12] has not identified the size of the irradiation spot on the retina, the characteristic radius of the irradiation spot on the retina $R_{s.r} \approx 40$ μm is calculated in order for the sizes of the predicted thermodenaturation lesion to agree with the sizes of experimental lesions. Figure 2 gives experimental [12] and numerical results for the energies $Q_{c.o}$ and $Q_{c.g}$ of radiation pulses on the monkey cornea. Experimental and theoretical values of the energy $Q_{c.o}$ are in satisfactory agreement. General rules of the behaviour of $Q_{c.o}$ and $Q_{c.g}$ are similar to Fig. 1 and motivated by the same physical reasons.

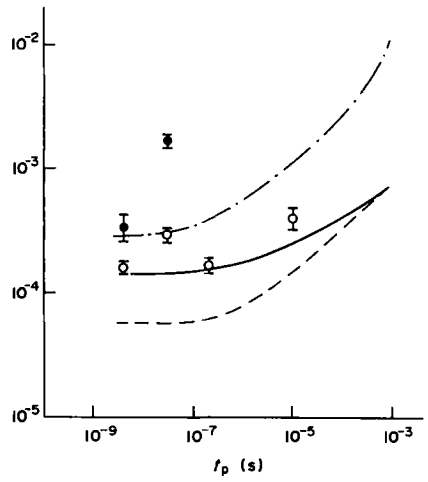

FIG. 2. The relationships of the calculated energies $Q_{c.v}$ (·—·—·), $Q_{c.o}$ (——), $Q_{c.g}$ (– – –) of radiation pulses with $\lambda = 1.06$ μm on the monkey cornea on t_p with the diameter of the irradiation spot on the retina $D_r = 2R_{s.r} \approx 80$ μm. Experimental energy values [7, 12]: (♦) pulse energy causing subretinal hemorrhage on the retina with probability 50%; and (♀) pulse energy causing the threshold retina damage with probability 50%.

One of the aims of the experimental study [12] was determining the dependence of $Q_{c.o}$ on t_p over the range $10^{-9} < t_p < 10^{-7}$ s. It was ascertained that the threshold $Q_{c.o}$ values at $t_p = 4 \times 10^{-9}$ and 2×10^{-7} s are about the same (only at $t_p = 3 \times 10^{-8}$ s are the $Q_{c.o}$ values about twice as large), which is verified by the calculated results. In the given case, the ratio of the threshold energies $Q_{c.o}/Q_{c.g}$ also reaches about 2–4. The R_0 values predicted using the theoretical energies $Q_{c.o}$ constitute, on average, about 12–15 μm; with the maximum biotissue temperature here being $T_m \sim 365$–380 K.

3. THERMOMECHANICAL EFFECT OF RADIATION ON THE GRANULES

With short and intense radiation pulses acting, the situation can arise where the thermal expansion rate of the heated biotissue proves to be commensurable with, or larger than, the speed of sound and a compression wave can be formed in the tissues. The originating pressures can be calculated by a simple model for a single granule. Water is used as the material modelling the properties of the granule and surrounding biotissue. This is due to the fact that water is the basic (amounting to about 80%) constituent of the eye media and its physical characteristics [14] resemble those of the eye tissues [11]. The characteristic relaxation time t_r of thermoelastic stresses resulting from a rapid heating and expansion of the granules is estimated by the equation $t_r \sim r_0/c_s$, where c_s is the speed of sound in water, and $t_r \sim 6 \times 10^{-10}$ s for $r_0 \sim 1$ μm. Consider the most interesting case with the affecting pulse duration $t_p \sim t_r$.

A calculation is conducted of the pressures originating under the action of short radiation pulses with $t_p = 10^{-9}$, 10^{-8} s and with predicted threshold energies $Q_{c.o}$. The maximum heating of a spherical granule $\Delta T_{0m} = T_{0m} - T_\infty$ by the end of the action of the short radiation pulse with $t_p = 10^{-9}$, 10^{-8} s, which allows granule heat exchange with the environment not to be taken into account, is equal to (see ref. [5])

$$\Delta T_{0m} = \frac{3E_{r0}K_{ab}}{4\rho_\infty c_0 r_0} \tag{3}$$

where E_{r0} is the energy density of radiation pulse on the retina. The average material density ρ in the region from r_0 to $r_f = r_0 + c_s t_p$ covered by the compression wave is

$$\rho = \rho_\infty \frac{V_f - V_0}{V_f - V_0 - \Delta V_0} \tag{4}$$

where ρ_∞ is the initial density, $V_0 = \frac{4}{3}\pi r_0^3$, $V_f = \frac{4}{3}\pi r_f^3$, and $\Delta V_0 = V_0 \beta \Delta T_{0m}$ is the granule volume increase due to thermal expansion, β is the thermal coefficient of volumetric expansion. The originating pressure p is predicted from the empirical equation of dynamic compressible water [15]

$$p = A\left[\left(\frac{\rho}{\rho_\infty}\right)^n - 1\right] \tag{5}$$

where $A = 3000$ atm and $n = 7$–8. The maximum granule heating ΔT_{0m}, which does not as yet give rise to a vapour bubble, should not be larger than $\Delta T_{0m} < 273$ K [16]. A calculation of p from equation (5) for $t_p = 10^{-9}$ s, $r_0 = 1$ μm, $\Delta T_{0m} \approx 273$ K yields $p \sim 1 \times 10^2$ atm. However, already at $t_p = 10^{-8}$ s and the threshold energy $Q_{c.o}$, the originating pressure constitutes $p \lesssim 1$ atm which is due to the corresponding volume increase V_r. Unfortunately, an exact criterion of the biotissue damage in the compression wave with a specific pressure drop is unknown. At the same time, it can be supposed that the pressure drop arising when $t_p \lesssim 10^{-9}$ s, by the action of a radiation pulse with a threshold (and overthreshold) energy value can bring about additional mechanical damage of the biotissues. It should be noted that at $t_p = 10^{-9}$ s and threshold pulse energies $Q_{c.g}$, which are about five times smaller than the energies $Q_{c.o}$, the originating pressure is, accordingly, about five times smaller and, apparently, counts little in the given case. With $t_p \gtrsim 10^{-8}$ s, and the threshold radiation pulse energies, the influence of mechanical damage, as follows from the results reported, is small.

4. THE FORMATION AND DYNAMICS OF A VAPOUR BLANKET ORIGINATING DURING THE INTERACTION OF RADIATION WITH A GRANULE

The publications [13, 17] treating the interaction of radiation with biotissues postulate that the biotissue heating of up to 100°C (373 K) results in cellular water evaporation (vapour generation) in the biotissue volume. Here, the possibility of water heating in the biotissue by short radiation pulses to markedly higher temperatures $T > 373$ K without vapour generation deep in the metastable region [16] is totally disregarded. At fairly short pulses of intense radiation, the granule and surrounding medium heating can occur at the rates of 10^8–10^9 K s^{-1}. In this case, the water surrounding the granule can get into the metastable state up to the temperature T_* of explosive ebullition capable of existing for a comparatively long time period in the water heating conditions, which is confirmed experimentally [16]. It must be pointed out that the possibility of the tissue heating beyond $T = 373$ K, as applied to the problem of the radiation effect on biotissues, is not touched upon. An intense homogeneous nucleation in overheated water around the granule begins, as predictions [18] made clear, on the water heating up to $T_* \approx 593$ K. Thereafter, a very rapid (explosive) ebullition of the water volumes occurs deep in the metastable region and the system goes into an equilibrium state characterized by the generation of a new phase, namely water vapour. A vapour blanket formed on the granule has an initial vapour pressure of about 10^2 atm which induces a subsequent rapid expansion of the vapour blanket. Thus, when radiation affects the pigmented biotissue layers containing granules, the new threshold radiation energy $Q_{c.v}$ can be introduced which causes granule surface heating to T_* and vapour interlayer formation on the granule. Here, vapour generation over the range $Q_{c.v}$–$Q_{c.o}$ can be neglected. The vapour blanket (the bubble) formation and expansion give rise to intense pressure waves [15] which result in mechanical damage and rupture of the biotissue.

This section reports on a theoretical study of the vapour blanket formation and dynamics with radiation pulses affecting an absorbing particle (granule) located in liquid.

Let a spherical particle of radius r_0 be situated in liquid (water) and from the initial instant of the optical radiation pulse action radiation energy absorption by the particle begins as well as heat exchange with the adjoining water layers which is described by the heat conduction equation

$$c_i \rho_i \frac{\partial T_i}{\partial t} = \frac{1}{r^2} \frac{\partial}{\partial r}\left(r^2 \kappa_i \frac{\partial T_i}{\partial r}\right) + q_i \qquad (6)$$

where T_i is the temperature, r is the radius of the spherical coordinate system with the origin fixed at the particle centre, t is the time, c_i, ρ_i, κ_i are the heat capacity, density and thermal conductivity, respectively, of the medium (those for $r \leqslant r_0$ ($i = 0$) are the particle parameters and those for $r > r$ ($i = 1$) are the liquid parameters), q_i is the power density of heat sources ($r \leqslant r_0$, $q_0 = IK_{ab}\pi r_0^2/V_0$, $V_0 = \frac{4}{3}\pi r_0^3$, K_{ab} is the efficiency factor of radiation energy absorption by the particle, $q_2 = 0$ for $r > r_0$). Phase transition (vapour generation) will only be considered in water surrounding the particle.

In the cases where nucleation due to contamination, etc. is absent and liquid is heated rapidly, a homogeneous nucleation mechanism with liquid deep in the metastable state is realized.

It is established that an intense homogeneous nucleation in water begins on heating beyond 578–590 K, after which a very explosive ebullition of water is observed and the system converts to an equilibrium state characterized by the generation of a new phase, namely vapour bubbles [16]. The presented evaluations revealed that, on reaching the temperature $T_* \approx 593$ K over the time of exposure to radiation pulse of duration $t_p \geqslant 10^{-8}$ s, at least more than one nucleus of the radius larger than the critical radius is formed in the heated water region around the microparticle and the explosive evaporation of liquid volumes deep in the metastable region occurs. Assume that the initial vapour layer around the particle originates instantaneously once its surface has reached the temperature $T_* = 593$ K during the explosive evaporation and the merging of critical nuclei. Here, the temperature of the vapour generated decreases to T_{10}, at which the homogeneous nucleation actually ceases. In this case, the pressure p_{10} and density ρ_{10} of the vapour are equal, correspondingly, to the pressure p_{1s} and density ρ_{1s} of saturated water vapour at the temperature T_{10}. The mass M_{10} of the vapour

blanket formed around the particle and its initial outer radius r_{10} are found from the mass and energy conservation law for the system under consideration and from the equation of the saturated vapour state

$$M_{20} = V_{20}\rho_2 = M_{10} = M_{10}\rho_{1s}(T_{10}) \quad (7)$$

$$4\pi\rho_2\int_{r_0}^{r_*} r^2 c_2(T)T(r)\,\mathrm{d}r = (p_{10}-p_\infty)(V_{10}-V_{20}) + 4\pi r_{10}^2\sigma + M_{10}(E_{10}+L_v) \quad (8)$$

$$p_{10} = p_{1s} = R_g\rho_{1s}(T_{10})T_{10} \quad (9)$$

where $r_* = r(T = T_*)$, $V_{10} = \frac{4}{3}\pi(r_{10}^3 - r_0^3)$, $V_{20} = \frac{4}{3}\pi \times (r_{20}^3 - r_0^3)$, $E_{10} = c_1 T_{10}$, c is the heat capacity, r_{20} is the outer radius of the water layer converting into vapour, R_g is the gas constant, σ is the surface tension coefficient, L_v is the vapour generated heat on a per-unit-mass basis, ρ is the density, p is the pressure, the subscripts 0, 1 and 2 refer to the particle, vapour and liquid, respectively. Energy equation (8) accounts for conversion of a part of the thermal energy of the overheated liquid layer into the work of the vapour blanket expansion to the volume V_{10}, for surface energy, thermal energy of vapour and energy expended on vapour generation. Solving the system of equations (7)–(9) with the known T_{10} value yields the original parameters for the vapour layer r_{10}, p_{10}, ρ_{10}, M_{10} which are used as the initial conditions in examining the vapour blanket dynamics in water.

The behaviour of the particle–vapour–liquid system is described by the following system of equations (see also refs. [19, 20])

$r \leqslant r_0$:

$$c_0\rho_0\frac{\partial T_0}{\partial t} = \frac{1}{r^2}\frac{\partial}{\partial r}\left(r^2\kappa_0\frac{\partial T_0}{\partial r}\right) + q_0 \quad (10)$$

for $r_0 < r \leqslant r_1$:

$$v_1(r,t) = -\frac{(r^3-r_0^3)}{3\gamma p_1 r^2}\frac{\mathrm{d}p_1}{\mathrm{d}t} + \frac{(\gamma-1)}{\gamma p_1}\left[\left(\kappa_1\frac{\partial T_1}{\partial r}\right)_r - \frac{r_0^2}{r^2}\left(\kappa_1\frac{\partial T_1}{\partial r}\right)_{r_0}\right] \quad (11)$$

$$p_1(t) = R_g\rho_1(r,t)T_1(r,t), \quad \frac{\partial p_1}{\partial r} = 0 \quad (12)$$

$$c_1\rho_1\left(\frac{\partial T_1}{\partial t} + v_1\frac{\partial T_1}{\partial r}\right) = \frac{1}{r^2}\frac{\partial}{\partial r}\left(r^2\kappa_1\frac{\partial T_1}{\partial r}\right) + \frac{\mathrm{d}p_1}{\partial t} + q_1 \quad (13)$$

$$\frac{\mathrm{d}p_1}{\mathrm{d}t} = -\frac{3\gamma\tilde{v}_1 p_1 r_1^2}{r_1^3 - r_0^3} + \frac{3r_1^2(\gamma-1)}{r_1^3-r_0^3}\left[\left(\kappa_1\frac{\partial T_1}{\partial r}\right)_{r_1} - \frac{r_0^2}{r_1^2}\left(\kappa_1\frac{\partial T_1}{\partial r}\right)_{r_0}\right] \quad (14)$$

$$\frac{\mathrm{d}r_1}{\mathrm{d}t} = \tilde{v}_1 + \tilde{j}/\tilde{\rho}_1 = \tilde{v}_2 + \tilde{j}/\tilde{\rho}_2 \quad (15)$$

$$\frac{\mathrm{d}M_1}{\mathrm{d}t} = 4\pi r_1^2\tilde{j}, \quad M_1 = 4\pi\int_{r_0}^{r_1} r^2\rho_1\,\mathrm{d}r \quad (16)$$

for $r_1 < r < \infty$:

$$v_2 = \tilde{v}_2 r_1^2/r^2 \quad (17)$$

$$\rho_2 = \text{const.} \quad (18)$$

$$c_2\rho_2\left(\frac{\partial T_2}{\partial t} + v_2\frac{\partial T_2}{\partial r}\right) = \frac{1}{r^2}\frac{\partial}{\partial r}\left(r^2\kappa_2\frac{\partial T_2}{\partial r}\right) + q_2 \quad (19)$$

$$r_1\frac{\mathrm{d}\tilde{v}_2}{\partial t} + \frac{3}{2}\tilde{v}_2^2 + \frac{2\tilde{j}\tilde{v}_2}{\rho_2} = \frac{p_1 - p_\infty - 2\sigma/r_1}{\rho_2} - 4\frac{\nu_2}{r_1}\tilde{v}_2 \quad (20)$$

where r_1 is the running outer radius of the vapour blanket, κ is the thermal conductivity, γ is the adiabatic exponent of water vapour, v is the velocity, $\tilde{j}$ the mass flux density of vapour and ν_2 the kinematic viscosity of water. The overscribed bar (see equation (22)) and tilde denote the quantities taken, correspondingly, at $r = r_0$ and $r = r_1$, the subscript ∞ refers to the initial value of the quantity.

The system of equations (10)–(20) involves heat conduction equations for the particle (10), vapour (13) and liquid (19), for the distribution of $v_1(r,t)$ (11) as well as the equation of the vapour state (12). Here, use is made of the homobaricity approximation $\partial p_1/\partial r = 0$, since the bubble expansion rate is much smaller than the speed of sound in vapour $\tilde{v}_1 \ll c_3$, as well as the equation for the vapour pressure p_1 (equation (14)), for the bubble radius r_1 (equation (15)), for the vapour mass M_1 (equation (16)), and the continuity equation for liquid (equation (17)) under its incompressibility approximation (equation (18)), which is valid for the pressure $p_2 \leqslant 10^3$ atm, as well as the Rayleigh–Lamb equation for the bubble expansion rate $\tilde{v}_2$ (equation (20)).

The initial and boundary conditions for equations (10)–(20) have the form

$$\text{for } t = 0: \quad T_0 = T_2 = T_\infty, \quad v_2 = 0:$$

$$t = t_*: \quad r_1 = r_{10}, \quad p_1 = p_{10},$$

$$\rho_1 = \rho_{1s}(T_{10}), \quad v_1 = 0, \quad v_2 = 0 \quad (21)$$

$$\left.\frac{\partial T_0}{\partial r}\right|_{r=0} = 0, \quad \tilde{v}_1 = 0,$$

$$-\left(\kappa_0\frac{\partial T_0}{\partial r}\right)_{r_0} = -\left(\kappa_1\frac{\partial T_1}{\partial r}\right)_{r_0}: \quad \bar{T}_0 = \bar{T}_1$$

$$\tilde{T}_1 = \tilde{T}_2, \quad \tilde{j}L_{ev} = -\left(\kappa_1\frac{\partial T_1}{\partial r}\right)_{r_1} + \left(\kappa_2\frac{\partial T_2}{\partial r}\right)_{r_1} \quad (22)$$

$$\tilde{j} = \alpha_{ev}\left(\frac{kT_2}{2\pi m_2}\right)^{1/2}(\tilde{\rho}_{1s} - \tilde{\rho}_1)$$

for $r \to \infty$:

$$T_2 = T_\infty, \quad v_2 = 0, \quad p_2 = p_\infty \quad (23)$$

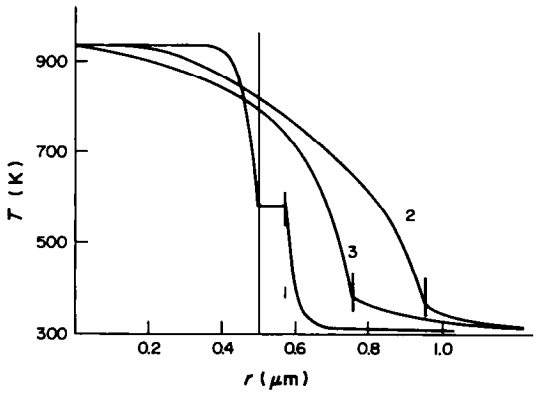

FIG. 3. The distribution of the temperature T along r at $t = 10^{-8}$ s (1), 6×10^{-8} s (2), and 1.2×10^{-7} s (3). A vertical line for $r = 0.5$ μm denotes the particle edge, vertical marks denote a location of the outer edge of the vapour blanket at the relevant time instant.

where α_{ev} is the condensation (evaporation) coefficient of water molecules and m_2 is the mass of water molecules. Here, account is taken of the temperature dependences of the surface tension coefficient and thermal conductivity of water and water vapour, and of the water evaporation heat.

A numerical simulation is performed for the vapour blanket formation and dynamics during the interaction of optical radiation pulses with an absorbing particle in water based on the solution of equations (6)–(23) on a computer using the Lagrange mass coordinates. Figures 3 and 4 give some calculated results for the interaction of radiation pulses of the duration $t_p = 10^{-8}$ s, constant radiation intensity $I_0 = \text{const.}$ during pulse at $I_0 K_{ab} = 1.775 \times 10^7$ W cm^{-2}, $q_1 = q_2 = 0$ with a particle of $r_0 = 0.5$ μm located in water. The $I_0 K_{ab}$ value is chosen such that the condition of the generation of the initial vapour blanket is fulfilled at the time instant of the pulse cessation, i.e. $t_* = t_p$. For simplicity, the values and temperature dependences of thermophysical parameters of the particle material are taken as those of water [21].

Figure 3 presents temperature distributions over r for several time instants. During the action of the pulse with $t_p = 10^{-8}$ s, heat exchange of the particle being heated with the environment results in pronounced temperature gradients on the particle edge. At the time instant $t = 10^{-8}$ s, an initial vapour blanket is generated of outer radius $r_{10} = 5.73 \times 10^{-5}$ cm, temperature $T_{10} = 578$ K and pressure $p_{10} = 9.18 \times 10^2$ N cm^{-2}, greatly in excess of the external pressure, $p_\infty = 1 \times 10^1$ N cm^{-2} which causes a subsequent expansion of the vapour blanket. Insofar as the particle heat exchange over the time t_p is small, the vapour blanket is surrounded by cold liquid which induces an intense vapour condensation on the liquid surface and a decrease in the vapour mass M_1 (see Fig. 4). In the course of time, particle heat exchange with the surrounding vapour and liquid develops, which induces the particle cooling. During the vapour blanket expansion, the vapour density decreases which results in condensation and in a certain stability of the vapour mass with time.

Figure 4 presents time dependences of the vapour pressure p_1, vapour mass M_1 and the outer radius of the vapour blanket r_1. With the vapour blanket expansion, r_1 increases up to a maximum value $r_1 \approx 9.8 \times 10^{-5}$ cm and the vapour pressure p_1 decreases to $p_1 \approx 6$ N cm^{-2} and a negative pressure drop between the vapour and the surrounding liquid is established. This causes a retardation of the outer edge of the vapour layer, its stopping and a reverse motion towards the particle surface. The vapour blanket contraction, in turn, induces a rise of the vapour density and pressure, which enhances the vapour condensation process and reduces the vapour mass M_1, when $t > 1.1 \times 10^{-7}$ s. The maximum expansion rate of the outer edge of the vapour blanket reaches about 1.5×10^3 cm s^{-1}, whereas the contraction rate of the outer edge of the blanket at the particle surface runs to about $(1.7\text{–}2) \times 10^3$ cm s^{-1}. The space–time distributions of the vapour density ρ_1, vapour velocity v_1 and liquid velocity v_2, etc. are obtained as well.

An analysis of the numerical results demonstrated that, with the vapour blanket contraction, the high-rate condensation and a sharp decrease in the vapour mass M_1, the vapour blanket can collapse. Here, as a consequence of the small thermal conductivity of the vapour, the particle is cooled slightly by the instant of

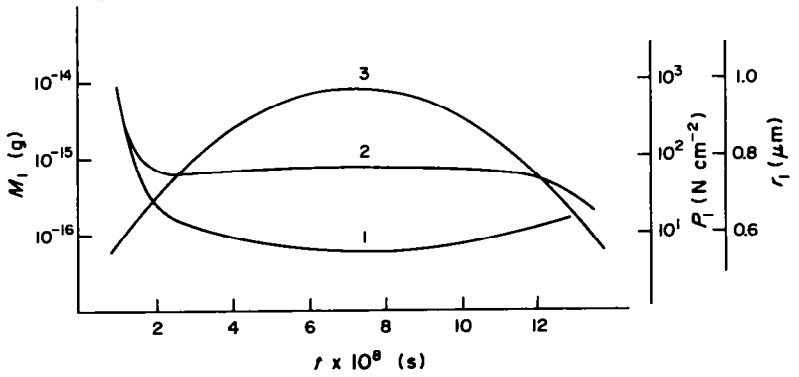

FIG. 4. The dependences of the vapour pressure p_1 (1), vapour mass M_1 (2) and outer radius of the vapour blanket r_1 (3) on t at $t_p = 10^{-8}$ s.

the vapour blanket collapse. As a result, the formation of a new vapour blanket with a subsequent recurrence of the process is possible after the vapour blanket collapse. On the other hand, at a slower decrease of the vapour mass due to condensation, there is a possibility that, under certain conditions, the vapour blanket begins to contract and expand periodically, rather than collapse.

Based on the results obtained, a calculation was performed for the threshold pulse energies $Q_{c.v}$ giving rise to the vapour blanket on the PE granules under the action of radiation pulses with $\lambda = 1.06$ μm at durations ranging from 10^{-3} to 10^{-8} s for the purpose of comparing them with experimental data [6, 7]; here the experiments [6, 7] registered the origination of vapour bubbles. Figure 2 gives experimental [6, 7] and numerical value of the threshold pulse energy $Q_{c.v}$ on the cornea. The experimental values of radiation energy [6, 7] conform to mechanical damage of the tissues and to subretinal hemorrhage from the choroid. The comparison of experimental and calculated energy values in Figs. 1 and 2 testifies the reasonable agreement, since the bubble formation in the retina tissues can cause the above-mentioned damage. A discrepancy between $Q_{c.v}$ and experimental value at $t_p = 3.5 \times 10^{-3}$ s in Fig. 1 and $t_p = 3 \times 10^{-8}$ s in Fig. 2, evidently results from the use of the indicated time dependences $I_0(t)$ and from the impossibility of taking into account the real peak temporal form of pulse [6, 7]. At $t_p = 3 \times 10^{-8}$ s, the pulse has a fine structure, which was noted in ref. [12], and this could be a possible reason for overestimating the experimental values of $Q_{c.o}$ and $Q_{c.v}$, as clear from Fig. 2. It must be remarked that $Q_{c.v}$ is only the smallest energy value (the lower limit) of the onset of bulk vapour generation. In the real conditions, however, the origination of vapour bubbles and mechanical ruptures would occur at pulse energies larger than $Q_{c.v}$. The dependence of $Q_{c.v}$ on t_p separates the pulse energy regions inducing evaporation, when $Q > Q_{c.v}$, and thermodenaturation with pressure waves without phase transition, when $Q < Q_{c.v}$ (see Figs. 1 and 2). With decreasing $t_p < 10^{-8}$ s, the radiation energies $Q_{c.v}$ and $Q_{c.o}$ converge, which can evidence a joint action of the outlined mechanisms in the damage lesion generation on the retina. In conclusion, ref. [22] should be noted which has studied the role of pigmented granules as laser rupture initiators and the origination of ionization waves in thermal explosion of the pigmented granules.

5. CONCLUSION

The current study has mathematically simulated thermal processes occurring during the interaction of optical radiation pulses with pigmented granules in heterogeneous layers of eye tissues. Mathematical models of the processes are given, numerical technical techniques are delineated and results of numerical calculations are reported. Concepts are introduced and the values of the threshold radiation pulse energies giving rise to a granular thermodenaturation lesion and to vapour generation on the granules are predicted. Consideration is given to the dynamics of a vapour blanket originating on the granule and to thermomechanical processes taking place during irradiation. The comparison of calculated results with experimental data and the agreement obtained validate the models and techniques developed. In the case in question, the mathematical simulation allows a thorough examination of the characteristics of thermal processes during and after irradiation, a realistic estimation of the biotissue damage mechanism (thermodenaturation, thermomechanical processes and bubble formation) and a correct interpretation of experimental results. The results obtained, including the ranges and values of radiation pulse energy taking certain effects upon exposure, are of considerable interest with regard to laser application in medicine (ophthalmology) for the purpose of substantiation and optimization of the irradiation regimes.

REFERENCES

1. M. Wolbarsht (Ed.), *Laser Application in Medicine and Biology*. Plenum Press, New York (1974).
2. D. Sliney and M. Wolbarsht, *Safety with Lasers and Other Optical Sources. A Comprehensive Handbook*. Plenum Press, New York (1982).
3. I. P. Sakina, A. E. Dontsov and M. A. Ostrovskiy, Melanin inhibition of the process of lipid photooxidation, *Biokhimya* **51**, 864–868 (1986).
4. V. K. Pustovalov and I. A. Khorunzhii, Selective interaction of short laser radiation pulses with pigmented biotissues with regard to their granular structure, *Kvantovaya Elektronika* **13**, 1461–1466 (1986).
5. V. K. Pustovalov and I. A. Khorunzhii, Thermal processes during the interaction of optical radiation pulses with heterogeneous laminated biotissues, *Int. J. Heat Mass Transfer* **33**, 771–783 (1990).
6. P. S. Avdeyev, Yu. D. Berezin, V. V. Volkov, Yu. P. Gudakovskiy, O. V. Konovalov, P. V. Preobrazhenskiy and R. V. Muratov, Biological effect of infrared laser radiation of 1.06 μm wavelength on the retina tissue, *Vestnik Oftalmologii* **1**, 26–30 (1982).
7. M. F. Blankenstein, J. A. Zuclich, R. G. Allen *et al.*, Retinal hemorrhage thresholds for *q*-switched Nd–Yag laser exposures, *Invest. Ophthalmology* **27**, 1176–1179 (1986).
8. M. V. Volkenshtein, *Biophysics*. Nauka, Moscow (1988).
9. A. J. Welch and G. D. Polhamus, Measurement and prediction of thermal injury in the retina of the rhesus monkey, *IEEE Trans. Biomed. Engng* **BME-31**, 633–644 (1984).
10. R. Birngruber, F. H. Hillenkamp and V.-P. Gabel, Theoretical investigation of laser thermal retinal injury, *Health Phys.* **48**, 781–796 (1985).
11. T. J. White, M. A. Mainster, J. H. Tips and P. W. Wilson, Chorioretinal thermal behavior, *Bull. Math. Biophys.* **32**, 315–322 (1970).
12. R. G. Allen, S. J. Thomas, R. F. Harrison, J. A. Zuclich and M. F. Blankenstein, Ocular effects of pulsed Nd laser radiation: variation of threshold with pulsewidth, *Health Phys.* **49**, 685–692 (1985).
13. A. J. Welch, The thermal response of laser irradiated tissue, *IEEE J. Quant. Electron.* **QE-20**, 1471–1482 (1984).

14. N. B. Vargaftik, *Handbook of the Thermophysical Properties of Gases and Liquids*. Nauka, Moscow (1972).
15. Ya. B. Zeldovich and Yu. P. Raizer, *Physics of Shock Waves and High-temperature Hydrodynamic Phenomena*. Nauka, Moscow (1966).
16. V. P. Skripov, *Metastable Liquid*. Nauka, Moscow (1972).
17. T. Haldorsson and V. Langerholc, Thermodynamic analysis of laser irradiation of biologic tissue, *Appl. Opt.* **17**, 3948–3958 (1978).
18. V. K. Pustovalov, I. A. Khorunzhii and D. S. Bobuchenko, The formation and dynamics of a vapour blanket originating during the interaction of radiation with a particle in liquid, *Izv. AN SSSR Ser. Fiz.* **52**, 1847–1851 (1988).
19. R. I. Nigmatulin, *The Fundamentals of Mechanics of Heterogeneous Media*. Nauka, Moscow (1978).
20. S. I. Zonenko, On the numerical investigation of dynamics of a vapour blanket near a heat solid particle submerged in liquid, *Izv. AN SSSR Mekh. Zhidk. Gaza* **4**, 154–158 (1985).
21. S. A. Rivkin and A. A. Aleksandrov, *Thermophysical Properties of Water and Steam*. Energiya, Moscow (1980).
22. V. S. Akopyan, Yu. K. Danileiko, L. P. Naumidi and A. M. Prokhorov, The damage mechanism of the drainage apparatus tissues in laser microsurgery of open-angle glaucoma, *Kvantovaya Elektronika* **14**, 1291–1298 (1987).